Journal of Materials Chemistry A

Accepted Manuscript

ROYAL SOCIETY OF CHEMISTRY

www.rsc.org/materialsA

Journal of Materials Chemistry A

Journal of Materials Chemistry A

Dynamic Article Links ►

Cite this: DOI: 10.1039/c0xx00000x

ARTICLE TYPE

www.rsc.org/xxxxxx

Porous Nitrogen and Phosphorus Co-doped Carbon Nanofiber Networks for High Performance Electrical Double Layer Capacitors

Guiyin Xu, Bing Ding, Jin Pan, Jinpeng Han, Ping Nie, Ye Zhu, Qi Sheng, Hui Dou*

Received (in XXX, XXX) Xth XXXXXXXXX 20XX, Accepted Xth XXXXXXXXX 20XX

DOI: 10.1039/b000000x

In this work, phytic acid is used as protonic acid dopant and soft template to synthesize 3D polyaniline (PANI) nanofiber networks. Then, the PANI nanofiber networks are transformed to porous nitrogen and phosphorus co-doped carbon nanofibers (P-NP-CNFs) by the carbonization and chemical activation process. P-NP-CNFs have a high specific surface area of 2586 $m^2 g^{-1}$ and large pore volume of 1.43 $cm^3 g^{-1}$, which are in favour of enhancing the electrochemical performance for electrical double layer capacitors. Moerover, the nitrogen and phosphorus doping in the carbon materials can increase the specific capacitance by a pseudocapacitive redox process. At a current density of 1 A g^{-1}, P-NP-CNFs show a large specific capacitance of 280 F g^{-1} and high specific capacitance retention of 94% after 10000 cycles. Especially, the phosphorus doping can broaden the electrochemical window to increase the energy density. Therefore, the energy density of symmetric capacitors based on P-NP-CNF is up to 22.9 Wh kg^{-1} at a power density of 325 W kg^{-1}, demonstrating P-NP-CNFs are superior electrode materials for electrical double layer capacitors.

Introduction

Renewable energies, such as solar, wind, tidal energy, are often intermittent and unreliable to satisfy the ever-increasing demands for electric automobile, unmanned aerial vehicle and portable electronic devices. Nowadays, electrical double layer capacitors (EDLCs) have attracted much attention because they can provide energy stably and quickly.[1-6] Moreover, EDLCs as energy storage devices possess high power density, low cost, long cycle life, and light weight.[7-9] Therefore, EDLCs are deemed to be one of the most promising energy storage devices for electronic equipment.[10-12]

However, the wide applications of EDLCs are restricted due to their low energy density.[13-15] Porous carbon materials have been explored to address the above issue, which show good electrochemical performance due to their high surface area, small ion-transport resistance and short diffusion distance.[16] However, the incompatibility of conductive pathways decreases the electrical conductivity of porous carbon materials along with the increase of porosity.[17] Thus, EDLCs based on porous carbon materials suffer from low specific capacitances at high current densities.

Recently, heteroatom-doped carbon materials have been considered as potential electrode materials for energy storage devices owing to their superior electrical conductivity, high surface activity and broad electrochemical window.[18, 19] Nitrogen-doped carbon materials, such as nitrogen-doped carbon nanotubes,[20] carbon nanofibers,[21] graphene,[22] carbon spheres,[23] and ordered mesoporous carbons,[24] have been demonstrated to exhibit high specific capacitances and excellent electrochemical stability for EDLCs. Nitrogen doping can cause a shift of the Fermi level to the valence band in carbon materials, thereby facilitating the electron transfer.[25] Moreover, the nitrogen incorporation can improve the wettability of carbon surface in the electrolyte and increase the capacitance by additional Faradaic redox.[26] Phosphorus doping into carbon materials can restrain the formation of unstable surface O-III groups to enhance oxidation stability at positive potential and adsorb hydrogen at negative potential.[27] Thus, phosphorus-doped carbon materials can widen the potential window to increase the energy density for EDLCs.[28] In addition, phosphorus doping can also increase the specific capacitance by the pseudocapacitance effect. However, the preparation of nitrogen and phosphorus-doped carbon materials are mainly based on NH_3, H_3PO_4, $(NH_4)_3PO_4$ activation methods, which require rigorous conditions and are time-consuming.[29-31] Thus, it is highly desirable to design a simple synthesis process to fabricate nitrogen and phosphorus co-doped carbon materials with proper pore-size distribution and high electrical conductivity for energy storage applications.

Herein, a simple and fast (several minutes) method was applied to synthesize the nitrogen and phosphorus co-doped carbon material precursor.[10, 11, 32] In the synthesis process, aniline was used as nitrogen source, phytic acid as dopant, phosphorus source and soft template to form 3D polyaniline (PANI) nanofiber networks. Then, a combined carbonization and chemical activation process in an inert gas was implemented to achieve porous nitrogen and phosphorus co-doped carbon nanofiber

networks (P-NP-CNFs). The interconnected 3D P-NP-CNFs have large surface area, unique pore-size distribution and excellent conductivity. Such unique structure of P-NP-CNFs combined with heteroatom-doping displays a remarkable electrochemical performance, demonstrating that P-NP-CNFs are promising electrode materials for EDLCs.

Experimental Section

Preparation of PANI, Nitrogen and Phosphorus Co-doped Carbon Nanofiber Networks (NP-CNFs) and P-NP-CNFs

To obtain 3D PANI nanofiber networks according to previous works,[11, 32] 1.842 mL phytic acid (50 wt% in water) was firstly dissolved in 4 mL distilled water. Then, 0.916 mL aniline was added into the phytic acid solution. Simultaneously, 0.572 g ammonium persulfate was dissolved in 2 mL distilled water. The temperature of these two solutions was reduced to 4 ℃ and quickly mixed afterwards. Lastly, the prepared PANI was immersed in distilled water for 24 hours to remove impurities and dried at 60 ℃ for 12 h.[32]

The obtained PANI as the carbon precursor was transferred to a tube furnace and heat-treated at 800 ℃ for 2 h under nitrogen with a heating rate of 5 ℃ min^{-1}. Then, the as-prepared sample was cooled to room temperature and NP-CNFs were obtained. NP-CNFs were dispersed in 3 M KOH ethanol solution and stirred for 6 hours (KOH/NP-CNFs weight ratio was 3:1). Then, the dried powder obtained by evaporating solvent was heated to 650 ℃ under nitrogen with a heating rate of 5 ℃ min^{-1} and kept at this temperature for 0.5 h. The activated sample was thoroughly washed with HCl (1 M) to remove any inorganic salts and then washed with distilled water until neutral pH. Finally, the activated carbon was dried under a vacuum atmosphere at 60 ℃ for 12 h and P-NP-CNFs were obtained.

Characterization

Field emission scanning electron microscopy (FESEM) and transmission electron microscopy (TEM) measurements were carried out with JEOL JSM-6380LV FE-SEM and FEI TECNAI-20, respectively. Scanning transmission electronic microscope (STEM) was performed on a Tecnai G2 F30. The X-ray photoelectron spectroscopy (XPS) analysis was performed on a Perkin-Elmer PHI 550 spectrometer with Al Kα (1486.6 eV) as the X-ray source. The N_2 adsorption/desorption tests were determined by Brunauer-Emmett-Teller (BET) measurements using an ASAP-2010 surface area analyzer. The pore size distribution (PSD) was derived from the desorption branch of the isotherm with the Barrett-Joyner-Halenda (BJH) method. Fourier transform infrared spectroscopy (FTIR) measurements were recorded on a Nicolet 750. Thermal gravimetric (TG) analysis was conducted on a TG-DSC instrument (NETZSCH STA 409 PC) under a N_2 atmosphere at a heating rate of 10 ℃ min^{-1} from 30 to 800 ℃.

Electrochemical Characterization

To measure the electrochemical properties of NP-CNFs and P-NP-CNFs-based supercapacitors, the working electrodes were prepared by mixing active material (5 mg), acetylene black and polytetrafluoroethylene (PTFE) binder with a weight ratio of 85:10:5. After coating the above slurry on foamed Ni grids (1 cm×1 cm), the electrodes were dried at 60 °C for several hours before pressing under a pressure of 15 MPa. Cyclic voltammetry (CV) and galvanostatic charge/discharge were investigated on CHI 660A electrochemical workstation (Shanghai Chenhua, China) in a conventional three-electrode system with 6 M KOH aqueous solution as the electrolyte. Platinum foil and a saturated calomel electrode (SCE) were used as counter and reference electrodes. Electrochemical impedance spectroscopy (EIS) was measured in the frequency range of 100 kHz-10 mHz with an amplitude of 5 mV. The specific capacitances are calculated from the galvanostatic charge/discharge curves based on the following equation:

$$C = \frac{I\mathrm{t}}{\mathrm{m}\Delta V}$$

where C, I, t, m and ΔV are the specific capacitance (F g^{-1}), the discharging current (A), the discharging time (s), the mass of active material (g) and the discharging potential range (V), respectively.

In the two-electrode system, the specific capacitances are calculated from the galvanostatic charge/discharge curves based on the following equation:

$$C = \frac{I\mathrm{t}}{\mathrm{m}\Delta V}$$

where C, I, t, m and ΔV are the specific capacitance (F g^{-1}), the discharging current (A), the discharging time (s), the total mass of electrode materials (including the acetylene black and binder) in both electrodes (g) and the discharging potential window (V), respectively.

The energy density and power density are calculated based on the following equations:

$$E = \frac{0.5 \times C \times (\Delta V)^2 \times 1000}{3600}$$

$$P = \frac{E}{t}$$

where E, C, ΔV, P and t are the energy density (Wh kg^{-1}), the specific capacitance (F g^{-1}), the discharging potential window (V), the power density (W kg^{-1}), the discharging time (s), respectively.

Results and discussion

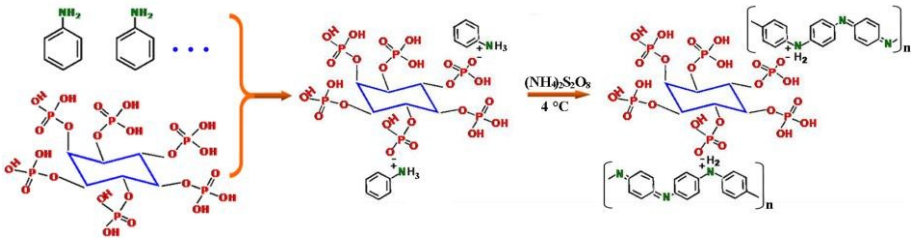

Figure 1. Schematic illustration for the reactive process of PANI nanofibers.

Phytic acid, also called inositol hexaphosphoric acid, is abundant and low cost as an organic phosphate compound extracted from the seeds of plants. Phytic acid can act as a dopant and play a soft-template role for the PANI morphological control.[32-35] Interestingly, the reaction only takes a few minutes from the brown solution of aniline and phytic acid to dark green PANI hydrogel (**Figure S1**). Based on the color and state changes of the reactive process, the possible schematic illustration is shown in **Figure 1**. Firstly, more than one aniline molecular reacts with phytic acid by protonation. Then, aniline polymerizes in the presence of $(NH_4)_2S_2O_8$ at 4 ℃ and turns to be phytic acid-doped 3D PANI nanofiber networks (**Figure 2a, d**). FTIR spectroscopy was carried out to demonstrate the successful doping of phytic acid into PANI (**Figure S2**). The absorption band at 3430 cm^{-1} is identified to the stretching vibration of O-H. The band at 2930 cm^{-1} is ascribed to the C-H bending mode from phytic acid. The bands at 1570, 1480, 1300 cm^{-1} are respectively attributed to the vibrations of quinoid ring, benzenoid ring in PANI, and C-O stretching in phytic acid.[36, 37] The band at 1140 cm^{-1} corresponds to the stretching of P=O and P=OOH.[27] Moreover, a band at 798 is due to the C-H bending mode from aromatic groups.

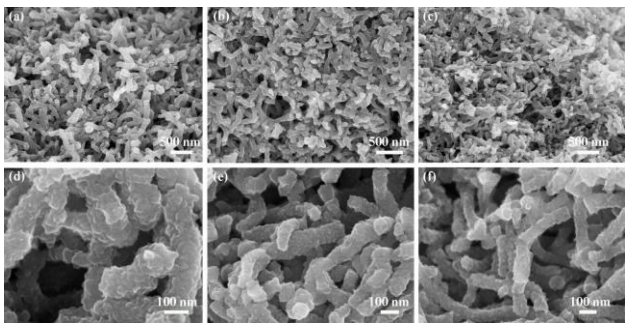

Figure 2. Scanning electron microscopy (SEM) images of (a, d) 3D PANI nanofiber networks, (b, e) NP-CNFs, and (c, f) P-NP-CNFs.

The phytic acid-doped 3D PANI nanofiber networks are suitable precursors for nitrogen and phosphorus co-doped carbon nanofiber networks. The yield of the obtained NP-CNFs from PANI nanofiber networks is up to 34.6% (**Figure S3**). After the carbonization, NP-CNFs maintain the 3D structure of PANI and the diameter has a little shrinkage compared with that of PANI (**Figure 2b, e**). For increasing the specific surface area and pore volume, the KOH chemical activation was employed to obtain P-NP-CNFs.[38] Importantly, P-NP-CNFs still remain the unique structure of PANI (**Figure 2c, f**). Such 3D nanofiber network structure can serve as the electrolyte reservoirs for EDLCs, thus shorten the transport pathway and facilitate ion transport. TEM was measured to further identify the morphology of NP-CNFs and P-NP-CNFs, clearly presenting 3D nanofiber networks (**Figure 3a, Figure S4**). High-resolution transmission electron microscopy (HRTEM) image reveals the presence of abundant worm-like micropores and mesopores in P-NP-CNFs (**Figure 3b**).[39] The distinctive pore distribution in P-NP-CNFs can allow the sufficient electrolyte infiltration, thus enabling accelerated ion transport and increasing the electrochemical performance for EDLCs. Carbon, nitrogen, oxygen and phosphorus are uniformly distributed in P-NP-CNFs as shown in the elemental mapping images (**Figure 3c**), demonstrating the successful preparation of nitrogen and phosphorus co-doped carbon nanofiber networks.

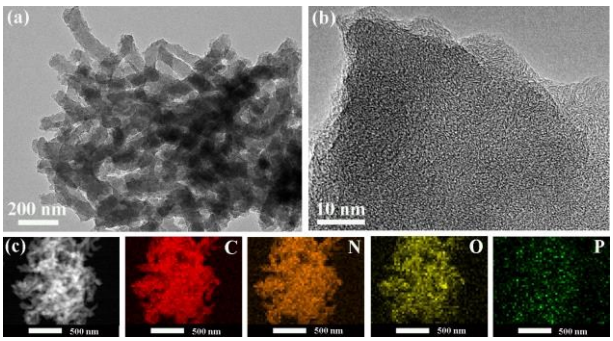

Figure 3. (a, b) TEM, (c) STEM images of P-NP-CNFs and corresponding elemental mapping images of carbon, nitrogen, oxygen and phosphorus.

The N_2 sorption isotherms at 77 K of NP-CNFs and P-NP-CNFs (**Figure 4a**) are a combination of Type I and Type IV, which are the characteristic of microporous and mesoporous materials. In the carbonization process of PANI nanofibers, the evaporation of H_2O, CO_2, CO *et al.*leaves porous structure in NP-CNTs. A clear uptrend at the low relative pressure (P/P_0<0.4) in the isotherms of NP-CNTs confirms that NP-CNTs are rich in micropores.[26] At the high relative pressure (P/P_0=0.4-0.9), the presence of significant hysteresis characteristics demonstrates that NP-CNTs have the mesoporous structure. Thus, the specific surface area of NP-CNFs (421 $m^2\ g^{-1}$) is increased compared with that of PANI nanofibers (26 $m^2\ g^{-1}$, **Figure S5**). After the KOH chemical activation, the specific surface area of P-NP-CNFs is 2586 $m^2\ g^{-1}$. The pore volume of P-NP-CNFs (1.43 $cm^3\ g^{-1}$) is greatly larger than that of NP-CNFs (0.18 $cm^3\ g^{-1}$, **Figure 4d**). Then, XPS was carried out to detect the nitrogen and phosphorus bonds for NP-CNFs and P-NP-CNFs. The amounts of nitrogen and phosphorus are 7.1%, 3.6% in NP-CNFs and 4.4%, 2.8% in P-NP-CNFs, respectively (**Table S1**). The nitrogen peaks of NP-CNFs and P-NP-CNFs can be matched into four peaks at 403.3,

401.0, 399.9 and 398.4 eV (**Figure 4b, e**),[40] which are identified to oxidized nitrogen (**N1**), the most stable quaternary nitrogen (**N2**, **Table S2**), pyrrolic nitrogen (**N3**), and pyridinic nitrogen (**N4**), respectively. The phosphorus peaks around 133.0 eV of NP-CNFs and P-NP-CNFs can be attributed to C-PO_3 and/or C-O-PO_3 groups (**Figure 4c, f**).[27, 30, 41] These XPS results further confirm the successful incorporations of nitrogen, phosphorus and corroborate well with the STEM analysis.

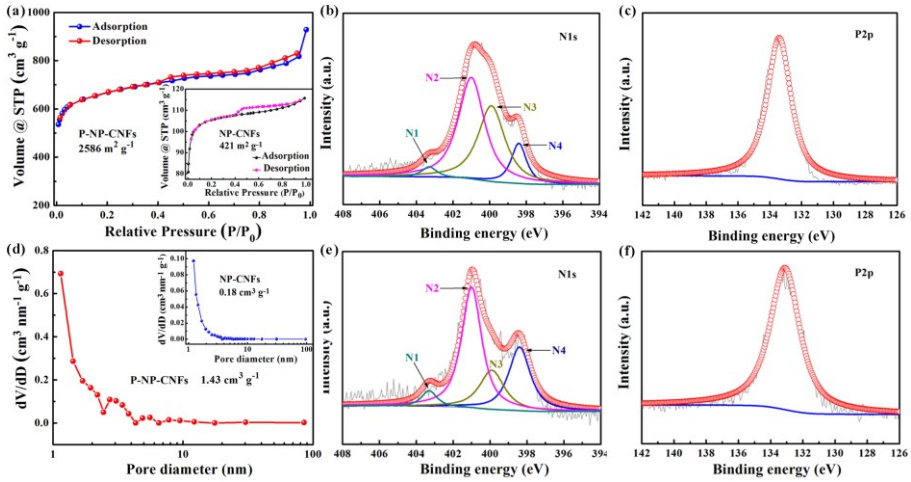

Figure 4. (a) N_2 adsorption-desorption isotherms at 77 K and (d) PSD curves of NP-CNFs and P-NP-CNFs. PSD is calculated using the Barrett-Joyner-Halenda method. (b) N1s and (c) P2p XPS spectra for NP-CNFs. (e) N1s and (f) P2p XPS spectra for P-NP-CNFs.

To evaluate the electrochemical performance of P-NP-CNFs as electrode materials for EDLCs, CV was carried out in a three electrode system in 6 M KOH aqueous solution. At low scan rates, the regular rectangular shapes in the CV curves of P-NP-CNFs are the typical characteristic of EDLCs (**Figure 5a**). Even while the scan rate is up to 100 mV s^{-1}, the CV curve still maintains the approximately rectangular shape, exhibiting rapid electron and ion transport. In addition, the inner area of the P-NP-CNFs CV curve is larger than that of NP-CNFs at the same scan rate (**Figure S6**), demonstrating the specific capacitance of P-NP-CNFs is effectively improved after the chemical activation process. In order to further evaluate the charge storage ability of the P-NP-CNFs electrode material, the galvanostatic charge/discharge measurement was carried out at different current densities (**Figure 5b**). The charge/discharge curves of P-NP-CNFs present isosceles triangular shapes, especially at high current densities, confirming the excellent charge/discharge properties of P-NP-CNFs for EDLCs.[23] A slight bend in these charge/discharge curves is resulted from the pseudocapacitance effect of nitrogen and phosphorus doping.[42] The IR drop of the P-NP-CNFs electrode at the initiation of the discharge curve is 0.021 V at a current density of 0.5 A g^{-1}, indicating a very low equivalent series resistance in EDLCs (**Figure S7**).[43, 44] Though NP-CNFs have a low pore volume and specific surface area, NP-CNFs show a high specific capacitance of 227 F g^{-1} at 1 A g^{-1} compared with previous reports (**Figure 5c, Table S3**).[45-47] The increased specific capacitance is attributed to the high content of nitrogen and phosphorus. However, the rate performance of NP-CNFs is unsatisfactory. When the current density is 20 A g^{-1}, the specific capacitance is just 94 F g^{-1}, which is only 41% of the initial specific capacitance. P-NP-CNFs combined 3D porous networks structure with the nitrogen and phosphorus co-doping (inset of **Figure 5d**) exhibit a high specific capacitance and favorable rate performance. At a current density of 1 A g^{-1}, the specific capacitance is up to 280 F g^{-1}. Even at a high current density of 20 A g^{-1}, the specific capacitance is 169 F g^{-1} and still remains 60% of the initial specific capacitance. Moreover, the specific capacitance retention of P-NP-CNFs is approximately 94% after 10000 cycles at a current density of 1 A g^{-1}, showing an excellent cycling stability (**Figure 5d**). These superior electrochemical results demonstrate that P-NP-CNFs can serve as a desired electrode material for EDLCs.

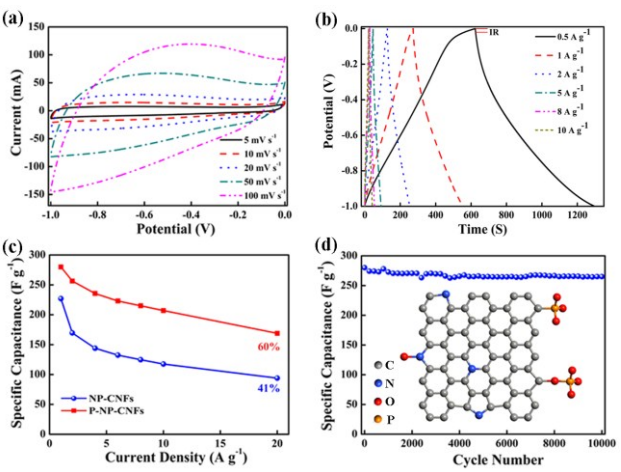

Figure 5. (a) CV curves of the P-NP-CNFs electrode in 6 M KOH aqueous solution at different scan rates. (b) The galvanostatic charge/discharge curves of the P-NP-CNFs electrode at different current densities. (c) The specific capacitances of NP-CNFs and P-NP-CNFs electrodes calculated from the discharge curves under different current densities. (d) Cyclic stability of the P-NP-CNFs-based EDLCs at a current density of 1 A g^{-1} (the inset is the schematic illustration for chemical structure of P-NP-CNFs).

The symmetric two-electrode EDLCs were assembled to further evaluate the electrochemical performance of P-NP-CNFs. Phosphorus doping can increase the stability of carbon electrodes in the aqueous electrolyte. The CV curves of P-NP-CNFs with different potential windows in the 6 M KOH aqueous solution were detected as shown in **Figure 6a**. The CV curve can maintain the quasi-rectangular shape with a potential window of 0-1.3 V,

indicating P-NP-CNFs have excellent capacitive performance. The specific capacitances of symmetric capacitors are calculated from the discharge curves under different current densities (**Figure 6b, Figure 6c**). At a current density of 0.5 A g^{-1}, the specific capacitance of P-NP-CNFs is 98 F g^{-1}, which is about two times as that of NP-CNFs (47 F g^{-1}). Moreover, the energy density of P-NP-CNFs is up to 22.9 Wh kg^{-1} at a power density of 325 W kg^{-1} (**Figure 6d**). Even at a high power density of 6500 W kg^{-1}, the energy density can still maintain 11.5 Wh kg^{-1}. The electrochemical performance of P-NP-CNFs exhibits better than that of NP-CNF, N-CNFs-900,[17] CNT,[48] and graphene/AC,[49] owing to the unique 3D network structure, large surface area, and nitrogen and phosphorus co-doping.

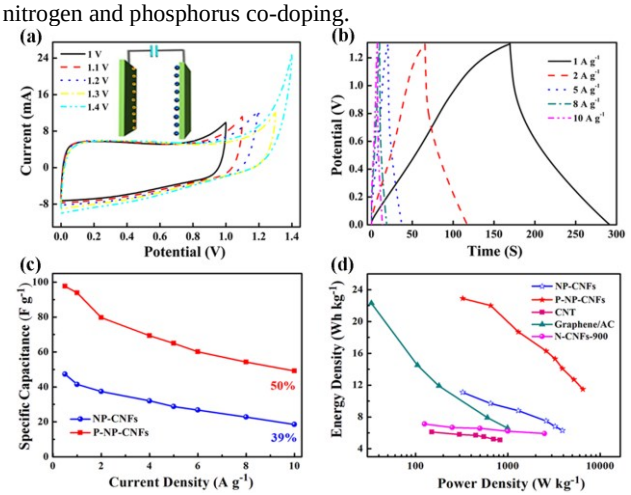

Figure 6. (a) CV curves of P-NP-CNFs with different potential windows at 10 mV s^{-1} (the inset is the schematic illustration of symmetric capacitors based on the P-NP-CNFs electrode). (b) The galvanostatic charge/discharge curves of symmetric capacitors based on P-NP-CNFs at different current densities. (c) The specific capacitances of symmetric capacitors based on NP-CNFs and P-NP-CNFs electrodes. (d) Ragone plots of symmetric capacitors based on carbon materials.

Conclusions

In summary, porous nitrogen and phosphorus co-doped carbon nanofiber networks have been successfully obtained by the carbonization and chemical activation of 3D PANI nanofiber networks. P-NP-CNFs have a high specific capacitance, excellent rate performance and cycling stability due to their large pore volume, high specific surface area, nitrogen and phosphorus co-doping. Importantly, the nitrogen and phosphorus co-doping can further increase the electrical conductivity, wettability of carbon materials, and have a pseudocapacitive effect. Therefore, P-NP-CNFs have a large specific capacitance of 280 F g^{-1} and high specific capacitance retention of 94% after 10000 cycles at a current density of 1 A g^{-1}. Meanwhile, P-NP-CNFs have a broader potential window due to the phosphorus doping. Therefore, the energy density of symmetric capacitors based on P-NP-CNFs is up to 22.9 Wh kg^{-1} at a power density of 325 W kg^{-1}, clearly demonstrating that P-NP-CNFs are outstanding candidates for EDLCs applications. Based on the superior electrochemical performance for EDLCs, P-NP-CNFs may be a promising candidate for lithium-air batteries, sodium-ion batteries and photocatalysis due to their unique 3D nanofiber structure and surface chemical properties.

Acknowledgements

The authors are grateful to the National Key Basic Research Program 973 (No. 2014CB239701), National Natural Science Foundation of China (No. 21173120, 51372116), Natural Science Foundation of Jiangsu Province (No. BK2011030, BK20151468, BK2011740), Fundamental Research Funds for the Central Universities of NUAA (NP2014403) and A Project Funded by the Priority Academic Program Development of Jiangsu Higher Education Institutions (PAPD). G.Y. Xu would like to thank Funding of Jiangsu Innovation Program for Graduate Education (KYLX15_0300) and Outstanding Doctoral Dissertation in NUAA (BCXJ15-07).

Notes and references

Jiangsu Key Laboratory of Material and Technology for Energy Conversion, College of Material Science and Engineering, Nanjing University of Aeronautics and Astronautics, Nanjing, 210016, P. R. China
E-mail: dh_msc@nuaa.edu.cn.
† Electronic Supplementary Information (ESI) available: [FTIR spectrum, TEM image, nitrogen adsorption-desorption isotherms, PSD, TG, and CV curves.] See DOI: 10.1039/b000000x/

1 Y. Zhu, S. Murali, M. D. Stoller, K. J. Ganesh, W. Cai, P. J. Ferreira, A. Pirkle, R. M. Wallace, K. A. Cychosz, M. Thommes, D. Su, E. A. Stach and R. S. Ruoff, *Science*, 2011, **332**, 1537-1541.
2 C. Merlet, B. Rotenberg, P. A. Madden, P. L. Taberna, P. Simon, Y. Gogotsi and M. Salanne, *Nat. Mater.*, 2012, **11**, 306-310.
3 L. F. Chen, Z. Y. Yu, J. J. Wang, Q. X. Li, Z. Q. Tan, Y. W. Zhu and S. H. Yu, *Nano Energy*, 2015, **11**, 119-128.
4 L. Shen, J. Wang, G. Xu, H. Li, H. Dou and X. Zhang, *Adv. Energy Mater.*, 2015, **5**, DOI: 10.1002/aenm.201400977.
5 L. F. Chen, Z. Y. Yu, X. Ma, Z. Y. Li and S. H. Yu, *Nano Energy*, 2014, **9**, 345-354.
6 D. R. MacFarlane, N. Tachikawa, M. Forsyth, J. M. Pringle, P. C. Howlett, G. D. Elliott, J. H. Davis, M. Watanabe, P. Simon and C. A. Angell, *Energy Environ. Sci.*, 2014, **7**, 232-250.
7 L. Wei, M. Sevilla, A. B. Fuertes, R. Mokaya and G. Yushin, *Adv. Funct. Mater.*, 2012, **22**, 827-834.
8 Y. Wang and Y. Xia, *Adv. Mater.*, 2013, **25**, 5336-5342.
9 P. Yang, Y. Ding, Z. Lin, Z. Chen, Y. Li, P. Qiang, M. Ebrahimi, W. Mai, C. P. Wong and Z. L. Wang, *Nano Lett.*, 2014, **14**, 731-736.
10 Y. Shi, L. Peng and G. Yu, *Nanoscale*, 2015, **7**, 12796-12806.
11 Y. Shi, L. Peng, Y. Ding, Y. Zhao and G. Yu, *Chem. Soc. Rev.*, 2015, **44**, 6684-6696.
12 Y. Shi, L. Pan, B. Liu, Y. Wang, Y. Cui, Z. Bao and G. Yu, *J. Mater. Chem. A*, 2014, **2**, 6086-6091.
13 L. Yuan, X. Xiao, T. Ding, J. Zhong, X. Zhang, Y. Shen, B. Hu, Y. Huang, J. Zhou and Z. L. Wang, *Angew. Chem. Int. Ed.*, 2012, **51**, 4934-4938.
14 N. Kurra, Q. Jiang and H. N. Alshareef, *Nano Energy*, 2015, **16**, 1-9.
15 J. Bae, M. K. Song, Y. J. Park, J. M. Kim, M. Liu and Z. L. Wang, *Angew. Chem. Int. Ed.*, 2011, **50**, 1683-1687.
16 D. W. Wang, F. Li, M. Liu, G. Q. Lu and H. M. Cheng, *Angew. Chem. Int. Ed.*, 2008, **120**, 379-382.
17 L. F. Chen, X. D. Zhang, H. W. Liang, M. Kong, Q. F. Guan, P. Chen, Z. Y. Wu and S. H. Yu, *ACS Nano*, 2012, **6**, 7092-7102.
18 N. S. Choi, Z. Chen, S. A. Freunberger, X. Ji, Y. K. Sun, K. Amine, G. Yushin, L. F. Nazar, J. Cho and P. G. Bruce, *Angew. Chem. Int. Ed.*, 2012, **51**, 9994-10024.
19 Z. Wang, Y. Dong, H. Li, Z. Zhao, H. Bin Wu, C. Hao, S. Liu, J. Qiu and X. W. Lou, *Nat. Commun.*, 2014, **5**.
20 G. Xu, B. Ding, P. Nie, L. Shen, J. Wang and X. Zhang, *Chem. Eur. J.*, 2013, **19**, 12306-12312.
21 W. Li, F. Zhang, Y. Dou, Z. Wu, H. Liu, X. Qian, D. Gu, Y. Xia, B. Tu and D. Zhao, *Adv. Energy Mater.*, 2011, **1**, 382-386.
22 H. Cao, X. Zhou, Z. Qin and Z. Liu, *Carbon*, 2013, **56**, 218-223.

23 J. Han, G. Xu, H. Dou and D. R. MacFarlane, *Chem. Eur. J.*, 2015, **21**, 2310-2314.

24 J. Wei, D. Zhou, Z. Sun, Y. Deng, Y. Xia and D. Zhao, *Adv. Funct. Mater.*, 2013, **23**, 2322-2328.

25 V. S. Veerasamy, J. Yuan, G. A. J. Amaratunga, W. I. Milne, K. W. R. Gilkes, M. Weiler and L. M. Brown, *Phys. Rev. B*, 1993, **48**, 17954-17959.

26 G. Xu, J. Han, B. Ding, P. Nie, J. Pan, H. Dou, H. Li and X. Zhang, *Green Chem.*, 2015, **17**, 1668-1674.

27 C. Wang, Y. Zhou, L. Sun, P. Wan, X. Zhang and J. Qiu, *J. Power Sources*, 2013, **239**, 81-88.

28 D. Hulicova-Jurcakova, A. M. Puziy, O. I. Poddubnaya, F. Suárez-García, J. M. D. Tascón and G. Q. Lu, *J. Am. Chem. Soc.*, 2009, **131**, 5026-5027.

29 R. Yang, G. Liu, X. Xu, M. Li, J. Zhang and X. Hao, *Biomass Bioenergy*, 2011, **35**, 437-445.

30 C. Wang, Y. Zhou, L. Sun, Q. Zhao, X. Zhang, P. Wan and J. Qiu, *J Phys Chem C*, 2013, **117**, 14912-14919.

31 Y. Qiu, W. Li, W. Zhao, G. Li, Y. Hou, M. Liu, L. Zhou, F. Ye, H. Li, Z. Wei, S. Yang, W. Duan, Y. Ye, J. Guo and Y. Zhang, *Nano Lett.*, 2014, **14**, 4821-4827.

32 L. Pan, G. Yu, D. Zhai, H. R. Lee, W. Zhao, N. Liu, H. Wang, B. C. K. Tee, Y. Shi, Y. Cui and Z. Bao, *Proc. Natl. Acad. Sci.*, 2012, **109**, 9287-9292.

33 D. Zhai, B. Liu, Y. Shi, L. Pan, Y. Wang, W. Li, R. Zhang and G. Yu, *ACS Nano*, 2013, **7**, 3540-3546.

34 Y. Zhao, B. Liu, L. Pan and G. Yu, *Energy Environ. Sci.*, 2013, **6**, 2856-2870.

35 Y. Shi, C. Ma, L. Peng and G. Yu, *Adv. Funct. Mater.*, 2015, **25**, 1219-1225.

36 L. Li, Z. Y. Qin, X. Liang, Q. Q. Fan, Y. Q. Lu, W. H. Wu and M. F. Zhu, *J Phys Chem C*, 2009, **113**, 5502-5507.

37 L. Mai, X. Xu, C. Han, Y. Luo, L. Xu, Y. A. Wu and Y. Zhao, *Nano Lett.*, 2011, **11**, 4992-4996.

38 J. W. F. To, Z. Chen, H. Yao, J. He, K. Kim, H. H. Chou, L. Pan, J. Wilcox, Y. Cui and Z. Bao, *ACS Cent. Sci.*, 2015, **1**, 68-76.

39 W. Luo, J. Schardt, C. Bommier, B. Wang, J. Razink, J. Simonsen and X. Ji, *J. Mater. Chem. A*, 2013, **1**, 10662-10666.

40 L. Qie, W. M. Chen, Z. H. Wang, Q. G. Shao, X. Li, L. X. Yuan, X. L. Hu, W. X. Zhang and Y. H. Huang, *Adv. Mater.*, 2012, **24**, 2047-2050.

41 J. Zhang, Z. Zhao, Z. Xia and L. Dai, *Nat. Nanotech.*, 2015, **10**, 444-452.

42 J. Tang, R. R. Salunkhe, J. Liu, N. L. Torad, M. Imura, S. Furukawa and Y. Yamauchi, *J. Am. Chem. Soc.*, 2015, **137**, 1572-1580.

43 Z. Wen, X. Wang, S. Mao, Z. Bo, H. Kim, S. Cui, G. Lu, X. Feng and J. Chen, *Adv. Mater.*, 2012, **24**, 5610-5616.

44 G. P. Hao, A. H. Lu, W. Dong, Z. Y. Jin, X. Q. Zhang, J. T. Zhang and W. C. Li, *Adv. Energy Mater.*, 2013, **3**, 1421-1427.

45 L. Sun, C. Tian, M. Li, X. Meng, L. Wang, R. Wang, J. Yin and H. Fu, *J. Mater. Chem. A*, 2013, **1**, 6462-6470.

46 X. Y. Chen, C. Chen, Z. J. Zhang, D. H. Xie and X. Deng, *Ind. Eng. Chem. Res.*, 2013, **52**, 10181-10188.

47 J. Han, G. Xu, B. Ding, J. Pan, H. Dou and D. R. MacFarlane, *J. Mater. Chem. A*, 2014, **2**, 5352-5357.

48 Q. Wang, Z. H. Wen and J. H. Li, *Adv. Funct. Mater.*, 2006, **16**, 2141-2146.

49 C. Zheng, X. Zhou, H. Cao, G. Wang and Z. Liu, *J. Power Sources*, 2014, **258**, 290-296.

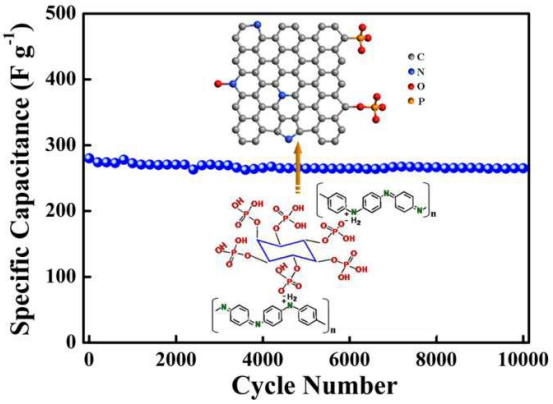

Porous nitrogen and phosphorus co-doped carbon nanofiber networks show excellent electrochemical stability for high performance electrical double layer capacitors.